Burned Area Mapping Using Unitemporal PlanetScope Imagery With a Deep Learning Based Approach

Ah Young Cho, Si-eun Park, Duk-jin Kim, *Senior Member, IEEE*, Junwoo Kim, Chenglei Li, and Juyoung Song

***Abstract*—The risk and damage of wildfires have been increasing due to various reasons including climate change, and the Republic of Korea is no exception to this situation. Burned area mapping is crucial not only to prevent further damage but also to manage burned areas. Burned area mapping using satellite data, however, has been limited by the spatial and temporal resolution of satellite data and classification accuracy. This article presents a new burned area mapping method, by which damaged areas can be mapped using semantic segmentation. For this research, PlanetScope imagery that has high-resolution images with very short revisit time was used, and the proposed method is based on U-Net which requires a unitemporal PlanetScope image. The network was trained using 17 satellite images for 12 forest fires and corresponding label images that were obtained semiautomatically by setting threshold values. Band combination tests were conducted to produce an optimal burned area mapping model. The results demonstrated that the optimal and most stable band combination is red, green, blue, and near infrared of PlanetScope. To improve classification accuracy, Normalized Difference Vegetation Index, dissimilarity extracted from Gray-Level Co-Occurrence Matrix, and Land Cover Maps were used as additional datasets. In addition, topographic normalization was conducted to improve model performance and classification accuracy by reducing shadow effects. The F1 scores and overall accuracies of the final image segmentation models are ranged from 0.883 to 0.939, and from 0.990 to 0.997, respectively. These results highlight the potential of detecting burned areas using the deep learning based approach.**

***Index Terms*—Burned area (BA) mapping, deep learning (DL), forest fire, PlanetScope, U-Net.**

I. Introduction

NATURAL wildfires are considered to play a significant role in clearing out forest litter on forest floors and allowing the soils to contain enough nutrients [1], [2], [3], [4], [5]. Despite these positive effects on the ecosystem, wildfires also cause some disadvantages, such as forest destruction, alteration of the water cycle, and social-economic damages, including huge losses of both life and property [6], [7], [8], [9]. Anthropogenic wildfires have happened and increased since fire has been used as a tool for human activities. Furthermore, the frequencies and spatial scales of wildfires have gotten higher and larger for a few decades due to climate change [10], [11], [12]. As a result, the drawbacks of wildfires outweigh the benefits. These days, it is not difficult to encounter stories of countries struggling with massive wildfires, for example, the massive wildfires in California and Australia [11], [13]. Most recently, Greece experienced the most severe heat wave in decades and these wildfires caused mass evacuations as the wildfires spread quickly despite attempts to extinguish them [14]. Wildfires are also a big emitter of greenhouse gases, and this would further fuel global warming. This situation is caught in a vicious circle. Thus, a necessity for wildfire management arises.

The Republic of Korea is also a country that needs effective wildfire management, especially forest fires. About 62.6% (6 286 000 ha) of the territory of the country is occupied with forests, so it has a vulnerable geographical feature to forest fires [15]. Even though the area of forest has decreased due to the change in land category, the Republic of Korea is the OECD's fourth-highest ratio of forest per land area [15]. According to statistics from the Korea Forest Service, 473 forest fires have occurred, damaging 1119 ha of land on average during the last ten-year period (2011–2020) [16]. With a relatively small land scale of South Korea, 99 646 km^2, this damage scale is considerable. The amount of significantly damaged forests caused by wildfires is immeasurable. Weather is also an influential factor in causing forest fires in both direct and indirect ways, on fire ignition potential, fire behavior, fire severity, and fire extinction, by promoting the radiative and convective heat transfer, increasing the dryness and flammability of the fuels and supplying oxygen to the combustion zone [17], [18], [19], [20], [21], [22], [23]. As a result, the most burning in Korea occurs with a marked dry season, especially in springs. The size of burnings is very varied, and the locations are distributed across the country. The government spends 34.1 million USD annually on efforts to prevent forest fires. In particular, approximately 5.2 million USD

Manuscript received 14 August 2022; revised 13 October 2022 and 14 November 2022; accepted 15 November 2022. Date of publication 28 November 2022; date of current version 7 December 2022. This work was supported in part by the Ministry-Cooperation R&D program of Disaster-Safety under Grant 20009742, funded by the Ministry of Interior and Safety (Korea), and in part by the Ministry of Science and ICT, Korea, under the Information Technology Research Center support program (IITP-2020-01424) supervised by the Institute for Information and Communications Technology Promotion. *(Ah Young Cho and Si-eun Park contributed equally to this work.) (Corresponding author: Duk-jin Kim.)*

The authors are with the School of Earth and Environmental Sciences, Seoul National University, Seoul 08826, South Korea (e-mail: panda772@snu.ac.kr; separk7447@snu.ac.kr; djkim@snu.ac.kr; darkcroa@snu.ac.kr; sengrea0926@snu.ac.kr; 96daniel@snu.ac.kr).

Digital Object Identifier 10.1109/JSTARS.2022.3225070

per 1010 hectares are spent annually on vegetation restoration and forest facility reconstruction in areas affected by forest fires [24]. Forest fires also pose a threat to local communities. In this sense, a risk management system is necessary to reduce damage from forest fires, and satellite technology can be a part of the solution.

Managing wildfires can be divided into three groups: before, during, and after a wildfire. Satellite data have been used for the whole stages of fire management. Remote sensing technology can be applied to these whole stages [25]. To bring a wildfire under control, early identification of the location and size of the fires is essential [26]. After the fire, postfire responses compromise mainly rehabilitation and restoration activities. These are long-term processes focusing on repairing infrastructure and natural resource damages caused by the fire and can take many years [27]. When it comes to the restoration of a fire, the mapping of burned areas (BA) is essential to rapid and effective recovery. In addition, BA information takes an important role in developing climate modeling and addresses international commitments related to carbon emissions [28]. Moreover, global BA products could be utilized to analyze fire effects, since only a few countries collect statics on BA and have reliable data [29].

To detect and estimate BA from wildfire, a few methods have been used, and manual field measurement has been a typical way to measure a scale and severity of a wildfire. However, using satellite imagery has been regarded as an effective and practicable way with the advancement of remote sensing satellite technologies, and it has some advantages. First, it is not easy and could be dangerous to access the fire-damaged area in person soon after the fire due to smoke and embers. On the other hand, a satellite can photograph the Earth's surface regardless of what disastrous situations happen. Next, in the event of a big forest fire, it is more effective to utilize satellite scenes for the measurement since the size of the BA is too extensive for expedite manual field measurement. With such advantages, much research has been conducted to find ways of more accurate BA mapping [30], [31], [32], [33].

However, utilizing satellite technology for mapping BA in optical imagery still has their limitation, such as the issue of atmospheric opacity, revisit time, and sensor characteristics. When a forest fire occurs, smoke from fire and cloud disturbs the observation of the BA, so when choosing scenes, only a few satellite imageries are valid for research [34]. Revisit time of a single satellite that provides global coverage is usually more than five days, and this acts as an obstacle since disasters have no fixed schedule [35]. That is to say that this feature would further retard obtaining pertinent satellite data. Moreover, as aforementioned, smoke from a fire and clouds in scenes narrow the possible options for research [36], [37], [38]. Recently, the increase in the number of satellites helps to solve this problem. Moreover, satellite constellations comprising a number of satellites overcome this limitation with rapid revisit times. Regarding the sensor issue, many satellites having coarse-resolution sensors have been used to measure BA, but it causes an underestimation of BA when fires are small [34]. These limitations are also compensated by the development of satellite remote sensing technology.

As many pieces of research have been conducted on the measurement of BA with satellite images, a lot of methods have been invented to analyze satellite data. Recently, research in this field welcomed dramatic progress thanks to deep learning (DL) approaches [39], [40]. Although the convolution neural network (CNN) algorithm was invented for analyzing medical classification tasks at first, it has also been proven that CNN is a useful tool for a satellite image classification method.

This study aims to find a practical model for measuring a BA of forest fires occurring in the Republic of Korea. As the occurrence of forest fires is repeated yearly, its management is important. Nevertheless, it does not seem that a high-performance detection model for Korean local forest fires has been developed yet. Therefore, devising a DL model to detect BA with satellite imagery would cast light on an immediate wildfire action plan. In addition, Korean forest fires have quite different characteristics compared to those of other countries due to their topographical features as aforementioned, and it could have some significant implications to develop a Korean own fire detection model. Through the research, we intended to answer the following questions: Which BA detecting model through DL is best suited to South Korea as a whole with a monotemporal approach using PlanetScope images? To get an answer to this question, we tried to find a band and index combination to bring the best result and additional information that could improve the result. Moreover, we considered developing an automated BA mapping algorithm to make it possible to use the research product in a real-life situation.

II. Study Area and Data Set

A. Study Area

According to a governmental forest fire statistics report from 2009 to 2018, the Republic of Korea has 432 forest fires a year, and roughly 70% of the forest fire damage occurred in spring due to its dry weather [41]. As moving into the 21st century, massive forest fires occurred more frequently due to climate change; for example, the number of forest fires in 2020 increased by 31% compared to the average of the last 10 years (474 cases), and the area of forest fire damage in 2020 increased by 161% compared to the average of the last 10 years (1120 ha) [16]. Based on the government statistics, 12 forest fire events happened in 9 areas (Andong, Ulsan, Goseong, Cheongsong, Busan, Gunwi, Samcheok, and Sangju) after 2017 were chosen as study areas considering the scales (larger than 31.9 ha) and availability of PlanetScope satellite data. The chosen forest fires' location, occurring date, and damaged area are shown in Table I.

B. Fire Data Set

1) PlanetScope: PlanetScope images were used for this research since PlanetScope, which is operated by PlanetLabs cooperation, provides high-resolution scenes with a very short revisit time that facilitates the acquisition of a daily image with worldwide coverage. As aforementioned, one of the limitations of using satellite images to map BA is coarse temporal resolution. As other satellites providing high-resolution images have

TABLE I
DESCRIPTION OF WILDFIRE EVENTS INVESTIGATED IN THIS WORK

	Location	Date	Damaged area (ha)
1	Dogye-eup, Samcheok-si, Gangwon-do	2017.05.06	765.12
2	Seongsan-myeon, Gangneung-si, Gangwon-do	2017.05.06	252
3	Sabulguk-myeon Sangju-si, Gyeongsangbuk-do	2017.05.06	86
4	Ganseong-eup, Goseong-gun, Gangwon-do	2018.03.28	356.85
5	Ubo-myeon, Gunwi-gun, Gyeongsangbuk-do	2018.08.15	31.9
6	Haeundae-gu, Busan	2019.04.02	56.9
7	Okgye-myeon, Gangneung-si, Gangwon-do	2019.04.04	1260.15
8	Toseong-myeon, Goseong-gun, Gangwon-do	2019.04.04	1266.62
9	Ulju-gun, Ulsan	2020.03.19	519
10	Pacheon-myeon, Cheongsong-gun, Gyeongsangbuk-do	2020.04.08	48.2
11	Pungcheon-myeon, Andong-si, Gyeongsangbuk-do	2020.04.24	1944
12	Toseong-myeon, Goseong-gun, Gangwon-do	2020.05.01	123.2

longer revisit times, PlanetScope overcomes the limitation by operating the PlanetScope constellation consisting of approximately 130 small CubeSat 3U satellites called "Dove" [42]. The PlanetScope imagery is known as having a spatial resolution of 3 m/pixel, but the images look a little less clear due to its unideal signal-to-noise ratio [43]. In addition, even though currently PlanetScope offers eight spectral bands, those products just have started to be obtainable. This is because PlanetScope has replaced old Dove satellites with the new generation Doves equipped with eight-band sensors since mid-March 2020. This replacement work was completed in August 2021 [44]. Consequently, the PlanetScope images used in this study are provided with four bands: blue (455–515 nm), green (500–590 nm), red (590–670 nm), and near infrared (NIR) (780–860 nm) with a color depth of 16 bits per channel [45].

For each study site, a cloud-free PlanetScope image was downloaded from planet.com (accessed in April 2021). We only downloaded images after the fire, since this research is focused on mapping BA using monotemporal PlanetScope imagery. PlanetScope images are offered as a Basic Scene product (level 1B), Ortho Scene product (level 3B), and an Analytic Ortho Tile product (level 3A) [45]. Between these three types of image products, we chose the second one, i.e., Ortho Scene product, with less than 5% cloud cover. This product is supplied with orthorectified and atmospheric correction (scaled Top of Atmosphere Radiance at the sensor). The Ortho Scene product has some benefits [46]. First of all, the imagery with orthorectification is the most effective to proceed value-added images such as land cover classification. Next, the PlanetScope offers images of which radiometric quality has been improved with radiometric correction.

The images used in this study were available and acquired closest to the date of the burn. When selecting the date of the scenes, cloud coverage and clarity of the BA perimeters of the preview images provided on the Planet website were considered (see Table II).

2) Labeling of the Damage and the Elaboration of the Reference Data: Under the machine learning process, it is necessary to generate input training data to find out what features each data has. This enables a computer to find a certain pattern or rule by analyzing the data by learning itself. Therefore, it is required to obtain labeling of the forest fire damage. Although some studies have used labeled samples provided by governmental institutions, we produced label data for this research due to the quality of publicly available spatial data. Since the range of pixel values of forest fire BA in satellite images varied from image to image, applying the same threshold value for the perimeter of the BA was not appropriate. Therefore, labels used in semantic segmentation were semiautomatically produced by adjusting the thresholds of the pixel value of the NIR band individually and gradually. In other words, we determined the appropriate threshold value by gradually changing the value for each image through visual interpretation. Also, it was possible to erroneously include various objects that are not BA but have similar pixel values of BA in the label. To lower it, the threshold value was applied only to the forest area

First, we clipped the BA out of the satellite images very roughly to reduce the possibility of creating false labels since there are several objectives in the scenes that have very similar pixel values. Then, we analyzed the pixel values of each PlanentScope scene to set appropriate thresholds. Comparing the perimeter of the created label of the damage to the original satellite image, the thresholds were adjusted. Even though the labeled samples were obtained through the process, there were still some labels that are not forest fire damage due to similar pixel values. As their size was much smaller than the forest fires, they were eliminated by setting the number of how many largest objects we would keep.

The ground truth masks were elaborated by manual digitizing of a satellite image. In this step, we created polygon vector layers based on the downloaded satellite imagery data. Then, each polygon was visually examined and modified with aerial images from Google Earth and other domestic mapping APIs. Lastly, we compared the areas of the polygons with the Korean government statics to evaluate the accuracy of ground truth data.

3) Additional Features—NDVI, GLCM Texture, and Land Cover Map: To meet better and more accurate results, additional datasets, the Normalized Difference Vegetation Index (NDVI), the dissimilarity extracted from Gray-Level Co-occurrence Matrix (GLCM), and the Land Cover Map were used.

In additional to spectral bands, spectral indices have been used to attain a more precise delineation of BA. Opinions vary on what spectral indices are suitable for mapping BA owing to the composition of land cover types, characteristics of sensors, and other factors. As a result, some studies recommended using NDVI based on their research [47], [48], whereas other indices, such as

TABLE II
PLANETSCOPE SATELLITE IMAGES FOR WILD FIRE DETECTION

Region	Acquisition time (UTC)	Satellite ID	Product level	Product type	Usage
Gangneung	21/05/2017 01:28:19	0e0e	3B	AnalyticMS	Training
Gangneung	21/05/2017 01:28:18	0e0e	3B	AnalyticMS	Training
Samcheok	29/05/2017 01:21:31	103a	3B	AnalyticMS	Test
Goseong	12/04/2018 01:37:58	1010	3B	AnalyticMS	Training
Goseong	12/04/2018 01:37:59	1010	3B	AnalyticMS	Training
Gangneung	08/04/2019 01:48:57	0f28	3B	AnalyticMS	Training
Goseong	07/04/2019 00:59:41	1050	3B	AnalyticMS	Training
Gangneung	08/04/2019 01:48:56	0f28	3B	AnalyticMS	Training
Goseong	07/04/2019 00:59:40	1050	3B	AnalyticMS	Training
Ulsan	23/03/2020 01:48:00	101f	3B	AnalyticMS	Training
Ulsan	23/03/2020 01:47:59	101f	3B	AnalyticMS	Training
Andong	27/04/2020 23:57:18	0f36	3B	AnalyticMS	Training
Andong	13/05/2020 01:50:22	1010	3B	AnalyticMS	Test
Goseong	06/05/2020 01:50:25	1025	3B	AnalyticMS	Test
Samcheok	29/05/2017 01:21:31	103a	3B	AnalyticMS	Training

normalized burn ratio [49], [50], normalized burned index [51], normalized difference moisture index [52], burn area index, and global environmental monitoring index [53], were considered a good spectral index to monitor and map wildfire events. Among these indices, we selected NDVI that can be calculated within the spectral bands of PlanetScope among indices that are mainly used for BA detection. One of the limitations of the PlanetScope constellation used in this study is that only four bands (red, green, blue, and NIR bands; no SWIR band) are on DOVE satellites. It narrowed down our options, and NDVI is the only index that can be extracted from the PlanetScope data. Therefore, we chose NDVI to achieve efficiency and accuracy. The NDVI is extracted using the following formula:

$$\text{NDVI} = \frac{(\text{NIR} - \text{Red})}{(\text{NIR} + \text{Red})}. \tag{1}$$

Next, GLCM is one of the texture analysis methods. Only four spectral bands were able to be used in this research, so we tried to find more auxiliary data to help make the result better. A set of eight different GLCM indicators (Contrast, Dissimilarity, Homogeneity, ASM, Energy, MAX, Entropy, GLCM Mean, GLCM Var, and GLCM Cor) were obtained by calculations based on the NIR band images. Among eight indicators, a few indicators demonstrating the most distinct difference between burned and unburned areas were chosen by visual interpretation: dissimilarity, entropy, homogeneity, and GLCM variance. In addition, some studies have shown that those four indicators are suitable for separating burned from unburned locations [54], [55], [56], [57].

Dissimilarity is one of the texture features calculated from GLCM and belongs to the contrast group. It is a measure of the difference in each element of the gray level and is more prominent when the local region has high contrast. Entropy is a measure of the irregularity of a histogram, and an image that visualizes 0 entropy would be seen as perfectly flat. In other words, entropy would be higher when the image has a more varied texture. GLCM variance shows the dispersion of parameter values around the mean of the combinations of reference and neighborhood pixels.

These three texture parameters can be calculated with the following equations:

$$\text{Dissimilarity} = \sum_{i,j\,=\,0}^{N-1} iP_{i,j}\,|i-j| \tag{2}$$

$$\text{Entropy} = \sum_{i,j\,=\,0}^{N-1} iP_{i,j}\,(-\ln P_{i,j}) \tag{3}$$

$$\text{Homogeneity} = \frac{\sum_{i,j\,=\,0}^{N-1} P_{i,j}}{1+(i-j)^2} \tag{4}$$

$$\text{Variance} = \frac{\sum_{i,j\,=\,0}^{N-1} (P_{i,j}-\mu)^2}{N-1} \tag{5}$$

where $P(i, j)$ is the frequency that two pixels occur in the image, one with gray level i and the other with gray level j.

Third, the Land Cover Map, which contains three types of forest (coniferous forest, broad-leaved forest, and mixed forest) is used to leave the final prediction result for the forest area. The forest in Korea is usually divided into coniferous forests, broad-leaved forests, and mixed forests [15]. Therefore, it is possible to extract only forest areas by using the Land Cover Map, and this makes BA mapping more efficacious.

III. METHODOLOGY

A. Topographic Normalization

In this research, we use a monotemporal approach to secure rapid data analysis and simplify the whole process. However, this approach has a critical problem caused by shadow. If some

shadows are included in satellite scenes, the shadows may cause false detection, especially in this research due to the limitation of the types of bands that can be used [36]. If we had chosen a multitemporal approach, it would have been way easier to reduce the effect of shadow. This is because the multitemporal method analyzes the difference in pixel value. Despite this disadvantage of the monotemporal approach, the benefits of the approach, such as rapid processing, seem amplified. As a result, we decided to apply a topographic normalization to each image for alleviating the shadow effect. Furthermore, in the case of Korea's topography, the forest is usually located in the mountains, which are so steep that it forms many shadows. This situation made this study perform topography normalization by the C-correction method [58], [59] to obtain the corrected image for alleviating the distortion of the real reflectance value of objects caused by topographic features. When taking into consideration that an automated BA detection algorithm would be developed, a modified C-correction method was necessary. Instead of using regression analysis in the original C-correction, we tried to find the value of C that minimized the standard deviation of ρ of each image.

B. Semantic Segmentation

CNN was first introduced as a new class of artificial neural networks for handwritten digit recognition [60]. CNN had improved a lot since then, and later a type currently used for DL was proposed [61]. Traditional filtering techniques used fixed filters to process images. However, CNN introduced a novel basic concept that "it automatically learns that each element of the filter expressed as a matrix is suitable for data processing." For example, when developing an image classification algorithm, the traditional method can be used. But one problem is that which filter to use in the algorithm should be determined through human intuition or iterative experimentation. Using CNN in this situation allows the algorithm to automatically learn the available filters for image classification. CNN and its modified version, such as fully convolutional network and U-net, have been applied to a variety of fields, and recently remote sensing domains also implement CNN to analyze image data to detect changes [62], [63], detect objects [64], [65], pan-sharpening and super-resolution [66], [67], and classify land cover [68], [69]. CNN, which is a type of DL model, is considered a promising method for BA segmentation since it makes it possible to learn any nonlinear function that maps its features and generalize the learned features [34].

We downloaded 17 PlanetScope scenes in total for the 12 forest fire events. Among the scenes, 16 satellite images were used to train, and one satellite image that was not used for training was used as the final validation data. The semantic segmentation was performed using the U-Net model. In the training process, 20% of the dataset is extracted randomly and used to measure the performance of the model, whereas the remaining 80% is used for training.

1) Finding an Optimal Patch Size: There is a chance that some boundaries of the images were confused with neighboring boundaries unless the full topological frame was given [70]. In other words, the model could not gain the whole context information, and this trend becomes more influential as the class size gets smaller [71]. However, a few studies have shown that the image would get blurry when using a too-big window size [72] or regions with inaccurate boundaries and classification of smaller fields would be included in other classes with larger patch size [73]. Therefore, three different patch sizes were tested in this research to determine the optimal patch size. The neural network we used requires that input data should be brought to a certain size. The original satellite images were divided into patches with sizes of 160×160, 256×256, and 480×480 to decide which patch size would have a better performance. We applied 2×2 padding to all tiles to detect features in the edges of the input for more accurate analysis. This tiling of satellite images is performed with python code. The model with 480×480 sized samples had to decrease its training batch size due to the limited quantity of graphic memory. There have been some studies showing that small batch sizes can cause more noise in the training gradients and a loss of generalizability. This can lead to less accuracy [74], [75]. However, the model trained with 160×160 sized samples made the worst result overall, although it was trained with a larger batch size than that of 480×480. The results of the models with 256×256 and 480×480 patch sizes showed similar results. A study also showed that for U-Net and ResUnet models which are only up to 256×256, improved results could be obtained by increasing the sample window size, even though this simultaneously decreases the training batch sizes [76]. Thus, the window size of the samples was decided as 256×256.

It was also tested which ratio of damage to no damage pixels brings better performance. The size of the largest forest fire events analyzed in this study is only 1944 ha, and even that of some forest fires is less than 100 ha. In other words, BA account for only a small portion of the entire satellite image (BA pixels/entire pixels = 0.0177). This means that using all images as training data can lead to the degradation of model performance due to class imbalance. Therefore, in this study, several tests with different proportions of damage to no damage pixels were performed. Finally, the test using images with a ratio of BA pixels of 10% to 90% in each patch were used as training data to mitigate the class imbalance problem. As a result, the ratio of the pixels (BA pixels/entire pixels) used for training increased to 0.42.

2) Data Augmentation: Input data augmentation's aims are usually regarded as increasing the amount of available training data and the robustness of the models to variations in the data [47]. The way of augmentation could be divided into two parts, i.e., geometric data augmentation and radiometric augmentation. In this study, rotation change and mirroring that belong to simple geometric image augmentation were applied to further increase the amount of training data four times. This augmentation was carried out with a multiple of 90°, which makes it possible that the augmented images are created without any pixel interpolation [47]. Besides rotations, mirroring also was applied, with the easiest forms being a flip along the vertical and a flip along the horizontal axis. As the final outcome, we could acquire a six times increase in the number of the training dataset.

3) Band Combination Test: Satellite sensors in the NIR domain and the shortwave infrared (SWIR) domain are usually understood as suitable sensors to detect BA [77], [78], [79]. This is because reflectance in the NIR domain would be declined considerably, while there has been a moderate increase of reflectance in the SWIR domain due to the dryness of postfire [80], [81]. This study used PlanetScope images which include the NIR band but no SWIR. In addition to the NIR band, there are still not many studies on which band combination is best if the red, green, and blue (RGB) bands are additionally used to detect BA. Since there are various factors that depend on the type of vegetation, season, and atmospheric conditions [53], [82], [83], spectral band combination tests were conducted to determine which bands should be used as the training material.

Among the available spectral bands (blue, green, red, and NIR), the NIR band is best at distinguishing between BA and unburned areas, even from the human eye, as previous accumulated studies have proven that using the NIR band is very suitable to detect BA and vegetation conditions [84]. At the same time, it is also possible to recognize BA with RGB images. Based on this, the test was conducted to find the best band combination that would enter the training with the NIR band.

In this step, all 17 satellite images were put into model training and predicted by the model. The performance of each band combination was assessed by three different criteria: F1 score, overall accuracy (OA), and IOU.

C. Masking With Land Cover Map

If satellite images are detected in the original size, the location of the forest fire does not require to be cut into the surrounding area by carefully identifying the location of the forest fire in advance, but there is a possibility that the sea, the reservoir will be misdetected as a forest fire area. Therefore, in this study, only detection results for mountainous areas were left using the Land Cover Map.

D. Accuracy Assessment

To evaluate the model, F1 scores, OA, intersection over union (IOU), and recall of the pixels classified as burned were calculated.

First, F1 score is a statistical measure of a model's accuracy. F1 Score is the weighted average of Precision and Recall. In this study, precision would be defined as the number of pixels that are in fact burned over that of detected burned pixels, while recall shows the ratio of the number of truly burned pixels to the number of pixels that should have been detected as truly burned pixels. The following equation shows how the F1 score is calculated:

$$\text{F1Score} = \frac{2 \times \text{precision} \times \text{recall}}{\text{precision} + \text{recall}} = \frac{\text{TP}}{\text{TP} + 0.5 \times (\text{FP} + \text{FN})} \tag{6}$$

where TP means true positive, TN is true negative, FP is false positive, and FN is false negative.

Next, OA means the number of correctly classified pixels over the total number of pixels. In other words, it yields misleading results. The equation for OA is defined as

$$\text{OA} = \frac{\text{TP} + \text{TN}}{\text{TP} + \text{TN} + \text{FP} + \text{FN}}. \tag{7}$$

IOU is also another accuracy measure. It is used to measure overlap between the predicted bounding box and the ground truth bonding box (the real object boundary)

$$\text{IOU} = \frac{\text{area of overlap}}{\text{area of union}}. \tag{8}$$

TABLE III
DL MODEL SCORES WITH DIFFERENT BAND COMBINATION TO COMPARE THE CONTRIBUTIONS OF RGB AND NIR BANDS (MEAN VALUES)

	F1	OA	IOU
4	0.746	0.72	0.512
123	0.72	0.704	0.488
1234	0.852	0.836	0.668

IV. RESULTS

A. Band Combination Test and Analysis

We conducted band combination tests to create an optimal BA mapping model. First, we tested DL models using every single band (red, green, blue, and NIR) to understand the sensitivity of each band to BA detection. As expected, the NIR single band model had the best scores on F1 score, OA, and IOU. However, the difference between the scores of NIR and other bands is not wide.

Besides BA are usually discernible in RGB images, so we trained a DL model with RGB bands and compared F1 score, OA, and IOU before all DL models that include the NIR band were tested. The scores of the DL model with RGB band are quite similar to that of the model including only the NIR band, as shown in Table III. Then, we also compared these two scores to that of the DL model that was trained on all available spectral bands of PlanetScope. At this time, the model trained with all possible four bands made the best performance. From this result, we supposed that the best model would contain the NIR band.

Next, we evaluated all DL models including the NIR band. The number of possible combinations when the NIR band must be included is 8. We compared F1 score, OA, and IOU of NIR to those of the models with all possible band combinations. The DL models were trained five times on a combination of a batch size of 16 patches. Fig. 1 summarizes the results of eight combinations of PlanetScope's four spectral bands (blue, green, red, and NIR).

As shown in Fig. 1, some DL model values run off the tracks. However, it was not easy to pick out a significantly good model. This is because the values are pretty much the same among the combinations. In addition, the rankings of the models' performances are varied over the criteria: each model's minimum value, maximum value, medium value, and mean value of the five DL models. Even if the criterion is fixed on one of those four criteria, the rank order of the F1 score, OA, and IOU are different. As stated above, this suggests that the NIR

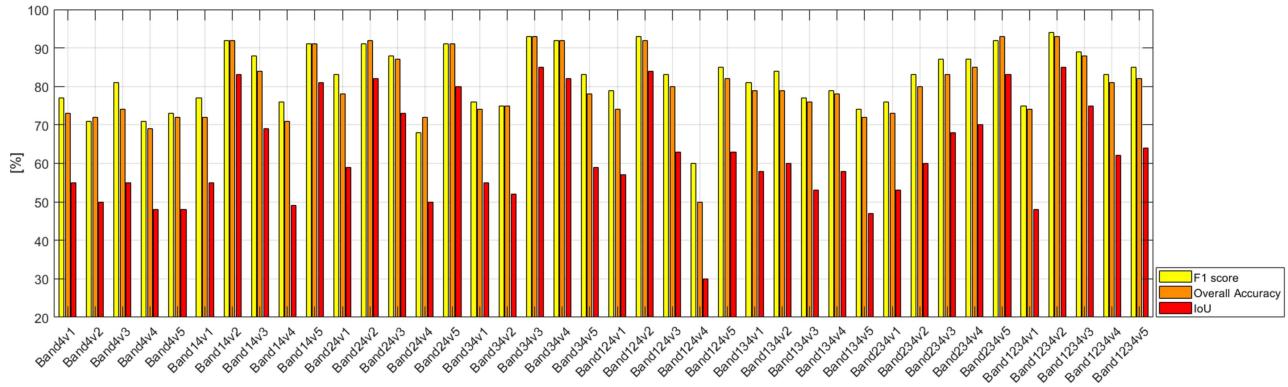

Fig. 1. Result of the band combination test (band1 = blue, band2 = green, band3 = red, band4 = NIR). The V (1,2,3,4,5) marked on the *x*-axis indicates the version number that showed the highest value among five runs.

TABLE IV
RESULTS OF THE DL MODELS WITH NDVI, GLCM, AND BLUE, GREEN, RED, AND NIR BANDS AS TRAINING DATA

Study area	Patch size	Mean of the 5 models	Standard deviation of the 5 models
(a) After topographic normalization			
Andong	256 × 256	F1Score: 0.930 IOU: 0.836 OA: 0.928	F1Score: 0.000 IOU: 0.005 OA: 0.004
Samcheok	256 × 256	F1Score: 0.938 IOU: 0.846 OA: 0.926	F1Score: 0.008 IOU: 0.022 OA; 0.015
Goseong	256 × 256	F1Score: 0.918 IOU: 0.824 OA: 0.920	F1Score: 0.050 IOU: 0.074 OA: 0.036
(b) Before topographic normalization			
Andong	256 × 256	F1Score: 0.924 IOU: 0.810 OA: 0.912	F1Score: 0.019 IOU: 0.050 OA: 0.022
Samcheok	256 × 256	F1Score: 0.928 IOU: 0.824 OA: 0.920	F1Score: 0.015 IOU: 0.035 OA: 0.018
Goseong	256 × 256	F1Score: 0.918 IOU: 0.812 OA: 0.904	F1Score: 0.019 IOU: 0.037 OA: 0.022

band is the most decisive for discrimination between burned and unburned areas. However, among them, the values of the five models using all four bands are spread out at least. Furthermore, we conducted naked eye distinction, if the performance score is similar to determine optimal band combination was determined by considering eye judgment and other situations. Under this circumstance, the models using all the bands map BA the best. Thus, we concluded that the optimal and most stable band combination is red, green, blue, and NIR.

Much of FP is an area that can be removed later using Land Cover Map, such as sea, reservoir, and lake. In addition, relatively G+NIR combination's prediction results showed that many areas were actually BA but were not detected.

B. Adding NDVI and GLCM (Dissimilarity)

Table IV shows the results of models with NDVI and GLCM (dissimilarity) in addition to Blue, Green, Red, and NIR bands as training data. To validate the effect of topographic normalization, we trained both input data applied modified C-correction and not applied. We also increased the batch size from 16 to 20 to get better performance. Unlike the spectral band combination

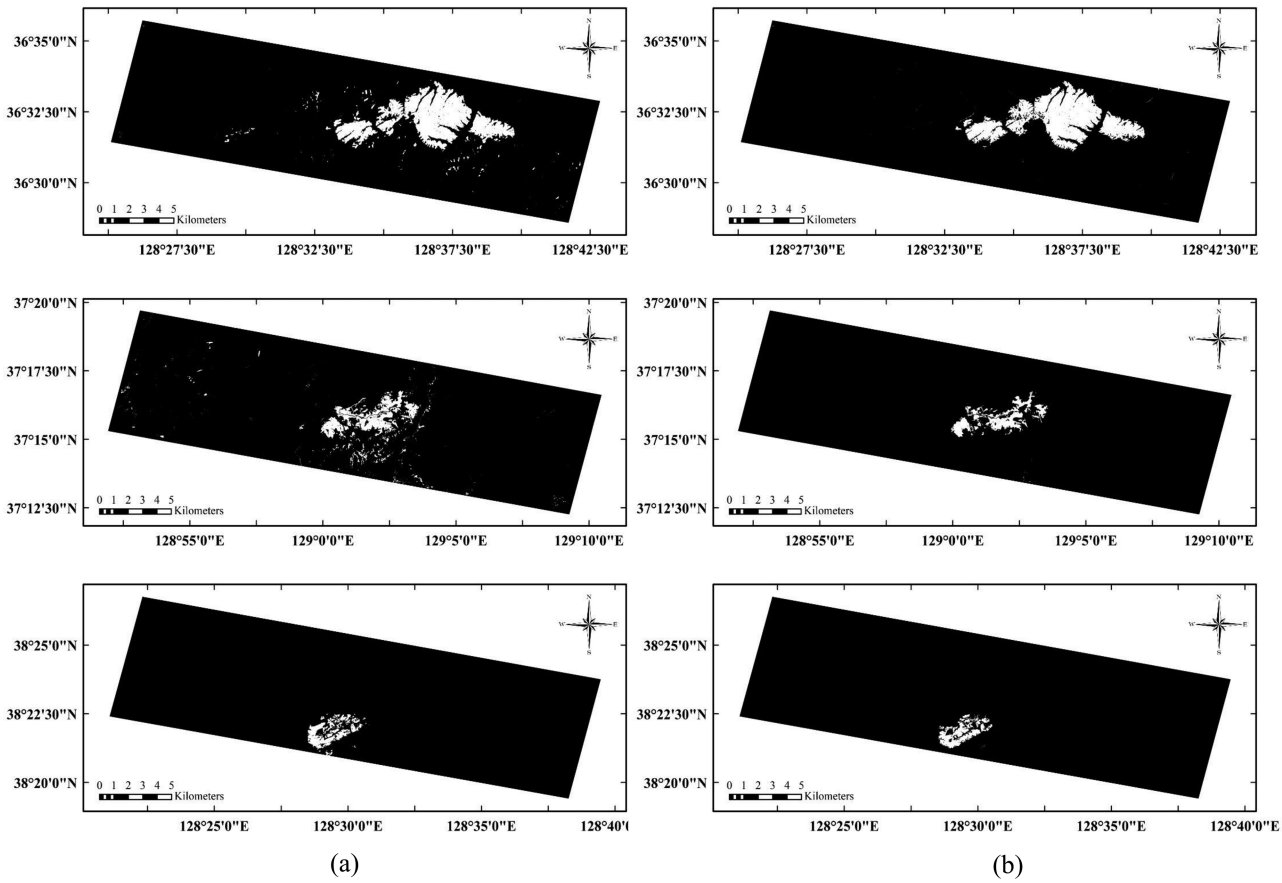

Fig. 2. Demonstration of the effectiveness of the topographic normalization process in removing terrain shadow effects. (a) Prediction results of the DL models without topographic corrections. (b) Prediction results of the DL models applied with the topographic corrections.

test, satellite images used for prediction were excluded from the training process to confirm the applicability of the model to other untrained regions with different vegetation or topographic features. To predict the BA of three satellite images (Andong forest fire in April 2020, Samcheok forest fire in May 2017, and Goseong forest fire in March 2018), these models were trained five times for each study area, and the conditions and the results of each model are summarized in Table IV. All other conditions are the same except for the difference between the satellite images used for training in the models.

Although the results vary slightly from model to model, the results are significantly improved compared to the scores of models previously trained with only spectral bands. As shown in Table IV, the scores of the topographic normalized group seem to excel more than those of not normalized group in the numbers.

Among these models, we chose a model that seems the optimal one and conducted the prediction process. According to Fig. 2 which shows the prediction results, we can see that commission errors induced by shadows are reduced.

C. Accuracy Assessment

After the prediction, we compared the prediction results with the ground-truth map. Three images in Fig. 3, right column show the comparison between predicting BA in the three regions and the ground-truth map after postprocessing using the Land Cover Map, while the images of the left columns are original image data of each area. The right column of Fig. 3 is only a part of the result, and the actual prediction was made for the entire size of the satellite image.

The label was directly produced based on several data surveys and reliable visual inspection was used as reference truth to validate the results. At this time, the F1 scores of models 1, 2, and 3 were 0.939, 0.883, and 0.889, respectively, which were less than the performance evaluation score of the model (see Table V). On the other hand, all the overall accuracies of models 1, 2, and 3 were measured much higher as 0.99, 0.997, and 0.996, respectively. These results imply that the predicted models have many more TN pixels and this affects the value of OA.

V. Discussion

In this study, we developed a DL-based BA mapping algorithm using only postfire PlanetScope imagery data. Before the semantic segmentation process, the terrain of satellite images was normalized. According to the model validation (see Table IV), topographic normalization showed positive effects on the model performance score to some extent. This is because we only trained the patches including both classes (burned and unburned) and excluded single-class tiles. In addition, the model was evaluated within the dataset. In other words, it is highly unlikely that patches having different pixel values because of the modified C-correction were included in the model training.

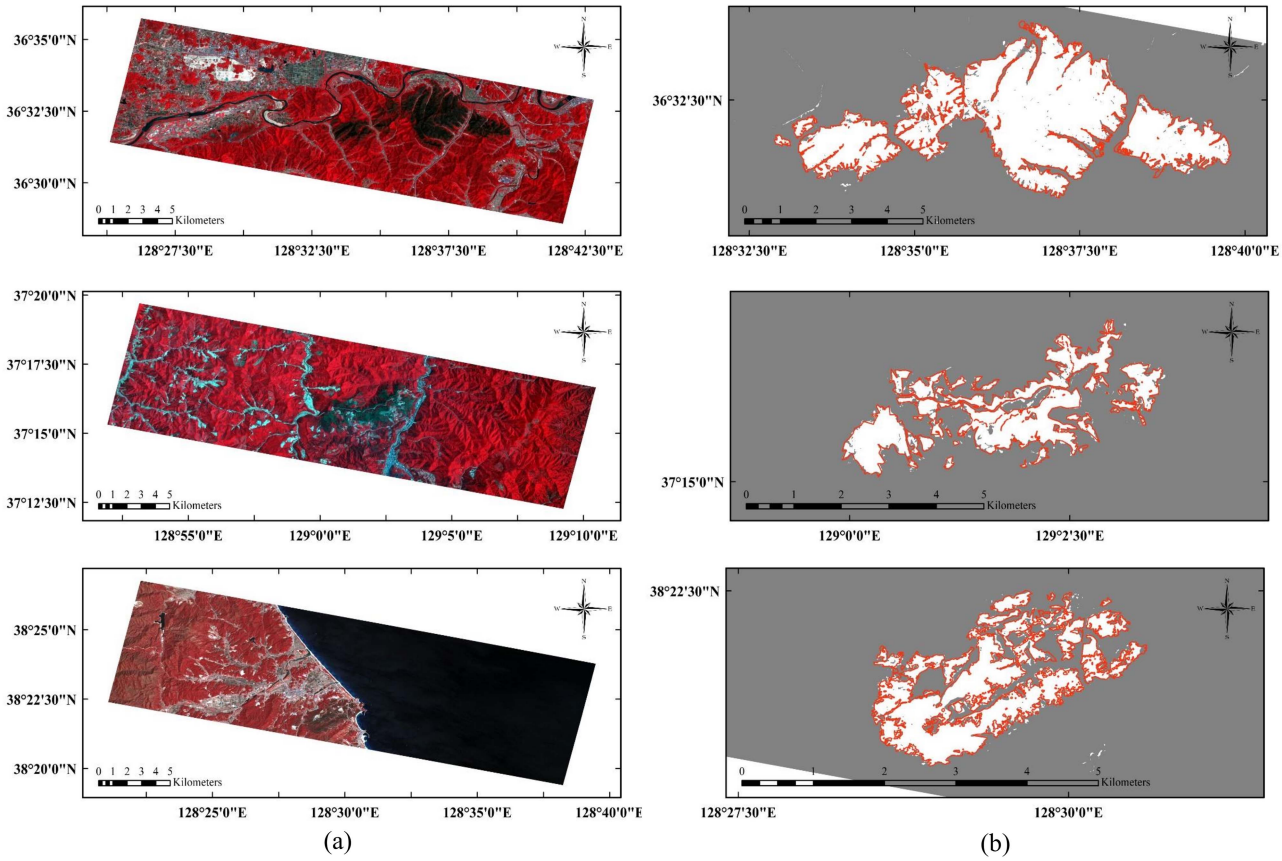

Fig. 3. BA mapping results of three areas that were randomly chosen among the study areas using U-Net segmentation methods with PlanetScope imagery data. (a) Original PlanetScope images of the three study areas. (b) Comparisons between the U-Net prediction of the BA (the white part of the figures) and the reference BA (the red line).

TABLE V
OVERVIEW OF THE ACCURACY ASSESSMENT FOR THE TESTING TILES (COMPARISON WITH A WHOLE PLANETSCOPE SCENE)

Model	Predicted Image	Trained Image	Patch size	The number of trainset	F1 score	IOU	Overall accuracy
1	Andong, 2020	Except Andong, 2020	256 × 256	822	0.939	0.886	0.99
2	Goseong, 2018	Except Goseong, 2018	256 × 256	918	0.883	0.791	0.997
3	Samcheok, 2017	Except Samcheok, 2017	256 × 256	892	0.889	0.801	0.996

As a result, the topographic normalization has some influence on the results of the accuracy assessment for the testing tiles.

In the DL stage, a U-Net model was used to conduct semantic segmentation. The ratio of BA and unburned area pixels was adjusted (approximately 4:6) to avoid problems caused by class imbalance. According to some studies, single-class tile integration helps the network to learn more about unburned areas, and consequentially reduces misclassification. However, not only is the extent of BA in our study very small to the original satellite images but also the types of unburned areas are various. That is why we did not try to include single-class tiles in the training stage. The fact that misclassification is rarely found in the prediction images justifies our decision.

Besides, through evaluation and comparison, the DL model using all four Red, Green, Blue, and NIR bands was selected as the optimal spectral band combination model. In the process of deciding the best band combination, we checked it again that NIR is very suitable for BA detection. At the same time, RGB bands also contain information that could assist in discrimination between burned and unburned areas. This result is thought to be because all four bands reflect well the changes in vegetation color and chlorophyll content caused by forest fires. Thus, when it comes to further development of satellite constellations comprised of many minisatellites, it would be a good idea that NIR sensors are equipped.

There is another implication of the band combination tests in our study. Although many studies try to find an optimal input data configuration that can acquire the best results with as few bands as possible to make the model lighter [29], PlanetScope imagery has only four spectral bands. In other words, decreasing

the number of the bands used in this study does not greatly serve to make a lighter model. In addition, we trained the DL model many times, and the models with more bands have lower deviations in the accuracy assessment.

When the values of the NDVI and the dissimilarity of the GLCM calculated from satellite data were used as input data, F1 score, OA, and IOU increased by about 0.1–0.2. As Fig. 2 shows, the topographic correcting method used in our research raises the accuracy of mapping algorithms, especially for Korea, a largely mountainous country. The end results were relatively accurate and neat so that the entire satellite image could be detected immediately without cropping the area around the forest fire based on a preliminary survey.

However, we should keep in mind that there are some limits, even though it shows the possibility that semantic segmentation is a promising method of rapid BA mapping. First of all, fire impacts on vegetation could not be clearly divided into burned and unburned areas. There are some factors that could influence BA conditions: the type of fire, fire behavior, and the time of the acquisition of postevent satellite images [29]. Therefore, it is not easy to determine where the perimeter of the BA is, and there is the possibility that the labels could be a little subjective depending on whom decided the threshold. Secondly, this study focused on developing a Korean forest fire mapping model, so the input data was limited. As a result, small fires were included in the input data to increase the number of training data sets.

VI. Conclusion

This study conducted a case study on Korea, where related studies were not sufficient, and showed the promising potential of using high-resolution images from PlanetScope and DL to detect BA.

Until now, there have been ample studies on wildfire detection and severity mapping using remote sensing. Most of the previous studies mainly used the multitemporal method, and there have been very few studies that try to develop a DL model using semantic segmentation methods [34], [85], [86], [87]. Our research, however, only used postfire images to develop a DL-based BA mapping algorithm using semantic segmentation methods. In addition, it has been very rare for studies to use PlaneScope's data because the constellation was first launched in 2016 and it is a commercial satellite. The number of available spectral bands is only four, and only the NIR band has the potential for detecting BA. Despite these limitations, the results of the accuracy assessment for the study areas are comparable to previous studies. This is because PlanetScope has some merit: PlanetScope has both high temporal and high spatial resolution. Therefore, we could use a relatively large number of high-resolution images as training input data by not missing the occurrence of wildfires. Moreover, even though PlanetScope has only four bands, the accuracy could be further improved by additionally using NDVI, GLCM, and land cover Map as input data for DL.

In addition, compared to previous studies, the number of study sites in our research is higher than many previous studies and we used the PlanetScope images of the diverse regions as training data. The accuracy assessment for the three random sites is similar and their performance scores of them are decent to apply this model to detect fire-damaged areas. This tells us that the transferability of our model is very high.

In the future, if the number of training data increases, the topographic normalization becomes better, and further studies on the indexes and GLCM that can indicate the BA conducted, the model will become more accurate and general.

Acknowledgment

The authors would like to thank Planet Labs for providing PlanetScope data via the E&R Program to DJK.

References

[1] L. H. Cammeraat and A. C. Imeson, "The evolution and significance of soil-vegetation patterns following land abandonment and fire in Spain," *Catena*, vol. 37, pp. 107–127, 1999.

[2] J. J. Martıńez-Sánchez, P. Ferrandis, J. de las Heras, and J. M. Herranz, "Effect of burnt wood removal on the natural regeneration of *Pinus halepensis* after fire in a pine forest in Tus valley (SE Spain)," *Forest Ecol. Manage.*, vol. 123, pp. 1–10, Oct. 1999.

[3] R. E. Vihnanek and T. M. Ballard, "Slashburning effects on stocking, growth, and nutrition of young Douglas-fir plantations in salal- dominated ecosystems of eastern Vancouver Island," *Can. J. Forest Res.*, vol. 18, no. 6, pp. 718–722, Jun. 1988.

[4] N. Caldararo, "Human ecological intervention and the role of forest fires in human ecology," *Sci. Total Environ.*, vol. 292, pp. 141–165, Jun. 2002.

[5] G. G. Ice, D. G Neary, and P. W. Adams, "Effects of wildfire on soils and watershed processes," *J. Forestry*, vol. 102, no. 6, pp. 16–20, Sep. 2004.

[6] H. A. Kramer, M. H. Mockrin, P. M. Alexandre, and V. C. Radeloff, "High wildfire damage in interface communities in California," *Int. J. Wildland Fire*, vol. 28, no. 9, pp. 641–650, Jul. 2019.

[7] J. M. Diaz, "Economic impacts of wildfire," *Southern Fire Exchange*, vol. 498, pp. 2012–2017, 2012.

[8] S. H. Doerr and C. Santín, "Global trends in wildfire and its impacts: Perceptions versus realities in a changing world," *Philos. Trans. Roy. Soc. B, Biol. Sci.*, vol. 371, no. 1696, Jun. 2016, Art. no. 20150345.

[9] C. Ichoku et al., "Biomass burning, land-cover change, and the hydrological cycle in Northern sub-Saharan Africa," *Environ. Res. Lett.*, vol. 11, no. 9, Sep. 2016, Art. no. 095005.

[10] J. T. Abatzoglou and A. P. Williams, "Impact of anthropogenic climate change on wildfire across western us forests," *Proc. Nat. Acad. Sci. USA*, vol. 113, no. 42, pp. 11770–11775, 2016.

[11] A. L. Westerling and B. P. Bryant, "Climate change and wildfire in California," *Climatic Change*, vol. 87, no. 1, pp. 231–249, 2008.

[12] M. A. Krawchuk, M. A. Moritz, M.-A Parisien, J. Van Dorn, and K. Hayhoe, "Global pyrogeography: The current and future distribution of wildfire," *PLoS One*, vol. 4, no. 4, Apr. 2009, Art. no. e5102.

[13] W. M. Jolly et al., "Climate-induced variations in global wildfire danger from 1979 to 2013," *Nature Commun.*, vol. 6, no. 1, pp. 1–11, Jul. 2015.

[14] D. Stougiannidou and E. Zafeiriou, "Wildfire economic impact assessment: An empirical model-based investigation for Greek agriculture," *Earth Syst. Environ.*, vol. 8, pp. 1–5, Oct. 2021.

[15] Korea Forest Service, "Statistical year book of forestry 2020 (in Korean)," Korea Forest Service, Daejeon, South Korea, 2021.

[16] Korea Forest Service, "Forest fires in Korea during the last ten-year period," 2020. Accessed: Jan. 18, 2021. [Online]. Available: https://www.forest.go.kr/kfsweb/kfi/kfs/frfr/selectFrfrStats.do?mn=NKFS_02_02_01_05

[17] R. P. Benson, J. O. Roads, and D. R Weise, "Climatic and weather factors affecting fire occurrence and behavior," *Develop. Environ. Sci.*, vol. 8, pp. 37–59, Jan. 2008.

[18] M. Migliavacca et al., "Modeling biomass burning and related carbon emissions during the 21st century in Europe," *J. Geophys. Res. Biogeosci.*, vol. 118, no. 4, pp. 1732–1747, Dec. 2013.

[19] D. Morvan and J. L. Dupuy, "Modeling the propagation of a wildfire through a Mediterranean shrub using a multiphase formulation," *Combustion Flame*, vol. 138, no. 3, pp. 199–210, Aug. 2004.

[20] M. G. Pereira, R. M. Trigo, C. C. da Camara, J. M. Pereira, and S. M. Leite, "Synoptic patterns associated with large summer forest fires in Portugal," *Agricultural Forest Meteorol.*, vol. 129, pp. 11–25, Mar. 2005.

[21] P. Pereira et al., "Spatial models for monitoring the spatio-temporal evolution of ashes after fire – A case study of a burnt grassland in Lithuania," *Solid Earth*, vol. 4, no. 1, pp. 153–165, May 2013.

[22] A. Venäläinen et al., "Temporal variations and change in forest fire danger in Europe for 1960–2012," *Natural Hazards Earth Syst. Sci.*, vol. 14, no. 6, pp. 1477–1490, Jun. 2014.

[23] Y. Kim, M. H. Jeong, M. Youm, and J. Kim, "Recovery of forest vegetation in a burnt area in the Republic of Korea: A perspective based on Sentinel-2 data," *Appl. Sci.*, vol. 11, no. 6, Jan. 2021, Art. no. 2570.

[24] E. Chuvieco, *Earth Observation of Wildland Fires in Mediterranean Ecosystems*. Berlin, Germany: Springer-Verlag, 2009.

[25] Y. Ban, P. Zhang, A. Nascetti, A. R. Bevington, and M. A. Wulder, "Near real-time wildfire progression monitoring with Sentinel-1 SAR time series and deep learning," *Sci. Rep.*, vol. 10, no. 1, 2020, Art. no. 1322.

[26] Y. G. Sahin and T. Ince, "Early forest fire detection using radioacoustic sounding system," *Sensors*, vol. 9, no. 3, pp. 1485–1498, 2009.

[27] A. C. M. Pessôa et al., "Intercomparison of burned area products and its implication for carbon emission estimations in the Amazon," *Remote Sens.*, vol. 12, no. 23, Nov. 2020, Art. no. 3864.

[28] E. Chuvieco et al., "Historical background and current developments for mapping burned area from satellite earth observation," *Remote Sens. Environ.*, vol. 225, pp. 45–64, 2019.

[29] P. Tsela et al., "Validation of the two standard MODIS satellite burned-area products and an empirically-derived merged product in South Africa," *Remote Sens.*, vol. 6, no. 2, pp. 1275–1293, Feb. 2014.

[30] F. M. De Araújo and L. G. Ferreira, "Satellite-based automated burned area detection: A performance assessment of the MODIS MCD45A1 in the Brazilian savanna," *Int. J. Appl. Earth Observ. Geoinf.*, vol. 36, pp. 94–102, Apr. 2015.

[31] Y. E. Shimabukuro, J. Miettinen, R. Beuchle, R. C. Grecchi, D. Simonetti, and F. Achard, "Estimating burned area in Mato Grosso, Brazil, using an object-based classification method on a systematic sample of medium resolution satellite images," *IEEE J. Sel. Topics Appl. Earth Observ. Remote Sens.*, vol. 8, no. 9, pp. 4502–4508, Sep. 2015.

[32] D. P. Roy and L. Boschetti, "Southern Africa validation of the MODIS, L3JRC, and GlobCarbon burned-area products," *IEEE Trans. Geosci. Remote Sens.*, vol. 47, no. 4, pp. 1032–1044, Apr. 2009.

[33] L. Knopp, M. Wieland, M. Rättich, and S. Martinis, "A deep learning approach for burned area segmentation with Sentinel-2 data," *Remote Sens.*, vol. 12, no. 15, 2020, Art. no. 2422.

[34] K. Ahmad et al., "Automatic detection of passable roads after floods in remote sensed and social media data," *Signal Process. Image Commun.*, vol. 74, pp. 110–118, May 2019.

[35] D. Stroppiana et al., "Integration of optical and SAR data for burned area mapping in Mediterranean regions," *Remote Sens.*, vol. 7, no. 2, pp. 1320–1345, Jan. 2015.

[36] P. Zhang, Y. Ban, and A. Nascetti, "Learning U-Net without forgetting for near real-time wildfire monitoring by the fusion of SAR and optical time series," *Remote Sens. Environ.*, vol. 261, Aug. 2021, Art. no. 112467.

[37] D. Hamilton, K. Brothers, C. McCall, B. Gautier, and T. Shea, "Mapping forest burn extent from hyperspatial imagery using machine learning," *Remote Sens.*, vol. 13, no. 19, Sep. 2021, Art. no. 3843.

[38] X. X. Zhu et al., "Deep learning in remote sensing: A comprehensive review and list of resources," *IEEE Geosci. Remote Sens. Mag.*, vol. 5, no. 4, pp. 8–36, Dec. 2017.

[39] L. Ma et al., "Deep learning in remote sensing applications: A meta-analysis and review," *ISPRS J. Photogrammetry Remote Sens.*, vol. 152, pp. 166–177, 2019.

[40] Korea Forest Service, "Statistical year book of forest fire 2020 (in Korea)," 2021.

[41] "PlanetScope," 2022. Accessed: Apr. 13, 2014. [Online]. Available: https://developers.planet.com/docs/data/planetscope/

[42] W. Deigele, M. Brandmeier, and C. Straub, "A hierarchical deep-learning approach for rapid windthrow detection on PlanetScope and high-resolution aerial image data," *Remote Sens.*, vol. 12, no. 13, Jul. 2020, Art. no. 2121.

[43] Planet Labs, "Understanding PlanetScope instruments last updated," Sep. 7, 2022. Accessed: Nov. 1, 2022. [Online]. Available: https://developers.planet.com/docs/apis/data/sensors/

[44] Planet, *Planet Imagery Product Specifications*. San Francisco, CA, USA: Planet Labs, 2021.

[45] Planet Labs, "Planet imagery product specification: PlanetScope & RapidEye," 2016. Accessed: Nov. 1, 2019. [Online]. Available: https://assets.planet.com/docs/combined-imagery-product-spec-april-2019.pdf

[46] D. Morresi, A. Vitali, C. Urbinati, and M. Garbarino, "Forest spectral recovery and regeneration dynamics in stand-replacing wildfires of central Apennines derived from Landsat time series," *Remote Sens.*, vol. 11, no. 3, Feb. 2019, Art. no. 308.

[47] E. A. Storey, D. A. Stow, and J. F. O'Leary, "Assessing postfire recovery of chamise chaparral using multi-temporal spectral vegetation index trajectories derived from Landsat imagery," *Remote Sens. Environ.*, vol. 183, pp. 53–64, Sep. 2016.

[48] J. C. White, M. A. Wulder, T. Hermosilla, N. C. Coops, and G. W. Hobart, "A nationwide annual characterization of 25years of forest disturbance and recovery for Canada using Landsat time series," *Remote Sens. Environ.*, vol. 194, pp. 303–321, Jun. 2017.

[49] J. Epting, D. Verbyla, and B. Sorbel, "Evaluation of remotely sensed indexes for assessing burn severity in interior Alaska using Landsat TM and ETM+," *Remote Sens. Environ.*, vol. 97, no. 1, pp. 92–115, Jun. 2005.

[50] K. S. Mpakairi, S. L. Kadzunge, and H. Ndaimani, "Testing the utility of the blue spectral region in burned area mapping: Insights from savanna wildfires," *Remote Sens. Appl. Soc. Environ.*, vol. 20, Nov. 2020, Art. no. 100365.

[51] E. H. Wilson and S. A. Sader, "Detection of forest harvest type using multiple dates of Landsat TM imagery," *Remote Sens. Environ.*, vol. 80, no. 3, pp. 385–396, Jun. 2002.

[52] F. Ngadze, K. S. Mpakairi, B. Kavhu, H. Ndaimani, and M. S. Maremba, "Exploring the utility of Sentinel-2 MSI and Landsat 8 OLI in burned area mapping for a heterogenous savannah landscape," *Plos One*, vol. 15, no. 5, May 2020, Art. no. e0232962.

[53] G. De Luca, J. M. Silva, and G. Modica, "A workflow based on Sentinel-1 SAR data and open-source algorithms for unsupervised burned area detection in Mediterranean ecosystems," *GISci. Remote Sens.*, vol. 58, no. 4, pp. 516–541, 2021.

[54] J. Lee, W. Kim, J. Im, C. Kwon, and S. Kim, "Detection of forest fire damage from Sentinel-1 SAR data through the synergistic use of principal component analysis and K-means clustering [Sentinel-1 SAR K-means clustering]," *Korean J. Remote Sens.*, vol. 37, no. 5/3, pp. 1373–1387, 2021.

[55] S. Arjasakusuma, S. S. Kusuma, Y. Vetrita, I. Prasasti, and R. Arief, "Monthly burned-area mapping using multi-sensor integration of Sentinel-1 and Sentinel-2 and machine learning: Case study of 2019's fire events in South Sumatra Province," *Indonesia Remote Sens. Appl. Soc. Environ.*, vol. 27, 2022, Art. no. 100790.

[56] E. S. Kim, S. H. Lee, and H. K. Cho, "Segment-based land cover classification using texture information in degraded forest land of North Korea," *Korean J. Remote Sens.*, vol. 26, no. 5, pp. 477–487, 2010.

[57] A. Shahtahmassebi, N. Yang, K. Wang, N. Moore, and Z. Shen, "Review of shadow detection and de-shadowing methods in remote sensing," *Chin. Geograph. Sci.*, vol. 23, no. 4, pp. 403–420, Aug. 2013.

[58] M. Kim, M. Jung, and Y. Kim, "Histogram matching of Sentinel-2 spectral information to enhance PlanetScope imagery for effective wildfire damage assessment," *Korean J. Remote Sens.*, vol. 35, no. 4, pp. 517–534, 2019.

[59] Y. LeCun et al., "Backpropagation applied to handwritten zip code recognition," *Neural Comput.*, vol. 1, no. 4, pp. 541–551, Dec. 1989.

[60] Y. Lecun, L. Bottou, Y. Bengio, and P. Haffner, "Gradient-based learning applied to document recognition," *Proc. IEEE*, vol. 86, no. 11, pp. 2278–2324, Nov. 1998.

[61] Q. Wang, X. Zhang, G. Chen, F. Dai, Y. Gong, and K. Zhu, "Change detection based on faster R-CNN for high-resolution remote sensing images," *Remote Sens. Lett.*, vol. 9, no. 10, pp. 923–932, 2018.

[62] E. Kalinicheva, J. Sublime, and M. Trocan, "Neural network autoencoder for change detection in satellite image time series," in *Proc. 25th IEEE Int. Conf. Electron. Circuits Syst.*, 2018, pp. 641–642.

[63] Y. Long, Y. Gong, Z. Xiao, and Q. Liu, "Accurate object localization in remote sensing images based on convolutional neural networks," *IEEE Trans. Geosci. Remote Sens.*, vol. 55, no. 5, pp. 2486–2498, May 2017.

[64] Y. Ren, C. Zhu, and S. Xiao, "Small object detection in optical remote sensing images via modified faster R-CNN," *Appl. Sci.*, vol. 8, no. 5, May 2018, Art. no. 813.

[65] D. E. Kislov and K. A. Korznikov, "Automatic windthrow detection using very-high-resolution satellite imagery and deep learning," *Remote Sens.*, vol. 12, no. 7, Apr. 2020, Art. no. 1145.

[66] K. M. Masoud, C. Persello, and V. A. Tolpekin, "Delineation of agricultural field boundaries from Sentinel-2 images using a novel super-resolution contour detector based on fully convolutional networks," *Remote Sens.*, vol. 12, no. 1, Dec. 2019, Art. no. 59.

[67] N. Kussul, M. Lavreniuk, S. Skakun, and A. Shelestov, "Deep learning classification of land cover and crop types using remote sensing data," *IEEE Geosci. Remote Sens. Lett.*, vol. 14, no. 5, pp. 778–782, May 2017.

[68] C. Tang, H. Chen, X. Li, J. Li, Z. Zhang, and X. Hu, "Look closer to segment better: Boundary patch refinement for instance segmentation," in *Proc. IEEE/CVF Conf. Comput. Vis. Pattern Recognit.*, 2021, pp. 13926–13935.
[69] J. Hamwood, D. Alonso-Caneiro, S. A. Read, S. J. Vincent, and M. J. Collins, "Effect of patch size and network architecture on a convolutional neural network approach for automatic segmentation of OCT retinal layers," *Biomed. Opt. Express*, vol. 9, no. 7, pp. 3049–3066, Jul. 2018.
[70] L. M. Zintgraf, T. S. Cohen, T. Adel, and M. Welling, "Visualizing deep neural network decisions: Prediction difference analysis," *CoRR*, vol. abs/1702.04595, pp. 1–10, Feb. 2017. [Online]. Available: http://arxiv.org/abs/1702.04595
[71] M. Pal, H. Rohilla, and B. C. Teja, "Patch based classification of remote sensing data: A comparison of 2D-CNN, SVM and NN classifiers," pp. 1–8, Jun. 21, 2020, *arXiv:2006.11767*.
[72] P. M. Radiuk, "Impact of training set batch size on the performance of convolutional neural networks for diverse datasets," *Inf. Technol. Manage. Sci.*, vol. 20, no. 1, Jan. 2017.
[73] I. Kandel and M. Castelli, "The effect of batch size on the generalizability of the convolutional neural networks on a histopathology dataset," *ICT Express*, vol. 6, no. 4, pp. 312–315, Dec. 2020.
[74] P. P. de Bem, O. A. de Carvalho Júnior, O. L. F. de Carvalho, R. A. T. Gomes, and R. F. Guimarães, "Performance analysis of deep convolutional autoencoders with different patch sizes for change detection from burnt areas," *Remote Sens.*, vol. 12, no. 16, Aug. 2020, Art. no. 2576.
[75] J. Norton, N. Glenn, M. Germino, K. Weber, and S. Seefeldt, "Relative suitability of indices derived from Landsat ETM+ and SPOT 5 for detecting fire severity in sagebrush steppe," *Int. J. Appl. Earth Observ. Geo-Inf.*, vol. 11, no. 5, pp. 360–367, Oct. 2009.
[76] L. Schepers, B. Haest, S. Veraverbeke, T. Spanhove, J. Vanden Borre, and R. Goossens, "Burned area detection and burn severity assessment of a heathland fire in Belgium using airborne imaging spectroscopy (APEX)," *Remote Sens.*, vol. 6, no. 3, pp. 1803–1826, Feb. 2014.
[77] M. Sali et al., "A burned area mapping algorithm for Sentinel-2 data based on approximate reasoning and region growing," *Remote Sens.*, vol. 13, no. 11, Jan. 2021, Art. no. 2214.
[78] P. Ceccato, S. Flasse, S. Tarantola, S. Jacquemoud, and J. M. Grégoire, "Detecting vegetation leaf water content using reflectance in the optical domain," *Remote Sens. Environ.*, vol. 77, pp. 22–33, Jul. 2001.
[79] E. Chuvieco, D. Riaño, F. M. Danson, and P. Martin, "Use of a radiative transfer model to simulate the postfire spectral response to burn severity," *J. Geophys. Res.*, vol. 111, no. G4, pp. G04S09–11–G04S09–15, Dec. 2006.
[80] A. V. Rocha and G. R. Shaver, "Advantages of a two band EVI calculated from solar and photosynthetically active radiation fluxes," *Agricultural Forest Meteorol.*, vol. 149, no. 9, pp. 1560–1563, Sep. 2009.
[81] T. Chen, R. Niu, P. X. Li, L. P. Zhang, and B. Du, "Regional soil erosion risk mapping using RUSLE GIS and remote sensing: A case study in Miyun Watershed North China," *Environ. Earth Sci.*, vol. 63, no. 3, pp. 533–541, Aug. 2010.
[82] R. Bokusheva, F. Kogan, I. Vitkovskaya, S. Conradta, and M. Batyrbayeva, "Satellite-based vegetation health indices as a criteria for insuring against drought-related yield losses," *Agricultural Forest Meteorol.*, vol. 220, no. 15, pp. 200–206, Apr. 2016.
[83] A. K. Brand and A. Manandhar, "Semantic segmentation of burned areas in satellite images using a U-net-based convolutional neural network," *Arch. Photogrammetry Remote Sens. Spatial Inf. Sci.*, vol. 43, pp. 47–53, Jun. 2021.
[84] X. Hu, Y. Ban Y, and A. Nascetti, "Uni-temporal multispectral imagery for burned area mapping with deep learning," *Remote Sens.*, vol. 13, no. 8, Jan. 2021, Art. no. 1509.
[85] F. H. Maskouni and S. T. Seydi, "Forest burned area mapping using bi-temporal Sentinel-2 imagery based on a convolutional neural network: Case study in Golestan forest," *Eng. Proc.*, vol. 10, no. 1, 2021, Art. no. 6.

Ah Young Cho received the B.Sc. degree in earth and environmental sciences and the J.D. degree in law from Seoul National University, Seoul, South Korea, in 2011 and 2014, respectively, and the LLM degree from Columbia University, New York, NY, USA, in 2019.

Before starting the LLM program at Columbia Law School, she was a Research Scientist and Lawyer for four years at the Ocean Policy Institute of Korea Institute of Ocean Science and Technology, a governmental research institute. In 2020, she joined the Institute of Basic Sciences, Seoul National University, Seoul, South Korea, as a Senior Researcher. Her current research focuses on marine environmental law and policy.

Si-eun Park is currently working toward the B.Sc. degree in earth and environmental sciences with Seoul National University, Seoul, South Korea.

Her research interests include disaster monitoring and mapping using satellite data.

Duk-jin Kim (Senior Member, IEEE) received the B.Sc. degree in earth system science and the M.Sc. and Ph.D. degrees in radar remote sensing and geophysics from Seoul National University, Seoul, South Korea, in 1999, 2001, and 2005, respectively.

From October 2005 to July 2007, he was a Postdoctoral Researcher with the University of Manitoba, Winnipeg, MB, Canada, and with the University of Michigan, Ann Arbor, MI, USA. From July 2007 to August 2008, he was a Senior Researcher with the Remote Sensing Division, Korea Aerospace Research Institute, Daejeon, South Korea. He is currently a Full Professor with the School of Earth and Environmental Sciences, Seoul National University. During his sabbatical leave from August 2014 to July 2015, he was a visiting scholar with the Radar Science and Engineering Section, NASA Jet Propulsion Laboratory, California Institute of Technology, Pasadena, CA, USA. His research interests include disaster monitoring using space-borne and airborne synthetic aperture radar systems (SAR), as well as environmental change monitoring using multitemporal and multisource SAR data.

Prof. Kim is a member of the Korean Institute of Electromagnetic Engineering and Science, Korean Society of Remote Sensing, and the Geological Society of Korea. He participated in the Steering Committee or Advisory Committee of many satellite programs in Korea (COMS, GEO-KOMPSAT-2B, and KOMPSAT-6/8).

Junwoo Kim received the B.Eng. degree in architecture from Yeungnam University, Gyeongbuk, South Korea, in 2011, the M.Sc. degree in remote sensing and GIS from Kyungpook National University, Daegu, South Korea, in 2014, and the Ph.D. degree in geography from the University of Leeds, Leeds, U.K., in 2019.

Between 2019 and 2021, he was a Senior Researcher with the Institute of Basic Sciences, Seoul National University, Seoul, South Korea. Since 2022, he has been a Research Professor with the SNU Future Innovation Institute, Seoul National University, Seoul, South Korea. His research focuses on broadening and deepening our understanding of the Earth and environments, and their interactions with human beings and society, using geospatial information technologies, such as remote sensing, GIS, and artificial intelligence.

Chenglei Li received the B.Sc. degree in geoscience and the M.Ed. degree in instructional program (geography) from Yanbian University, Yanji, China, in 2018 and 2020, respectively. He is currently working toward the Ph.D. degree in earth and environmental sciences with Seoul National University, Seoul, South Korea.

His research interests include marine oil spill detection and glacier calving front monitoring using deep learning technologies.

Juyoung Song received the B.Sc. and M.Sc. degrees in earth and environmental sciences in 2019 and 2021, respectively, from Seoul National University, Seoul, South Korea, where he is currently working toward the Ph.D. degree in radar remote sensing and geophysics.

His research interests include vessel monitoring using synthetic aperture radar, artificial intelligence, and radar signal processing.